ELSEVIER

Cement & Concrete Composites 21 (1999) 349–359

Cement & Concrete Composites

Micromechanical modeling of crack-aggregate interaction in concrete materials

Ashraf Ragab Mohamed, Will Hansen *

Department of Civil and Environmental Engineering, 2340 G.G. Brown Building, Ann Arbor, MI 48109-2125, USA

Received 4 September 1997; accepted 24 November 1997

Abstract

A new condition for crack penetration into the aggregate phase in concrete materials is developed based on numerical simulations. The numerical simulation utilizes a newly developed micromechanical model which considers the concrete internal structure as a three-phase material, viz. matrix, aggregate and interfaces between them. The micromechanical model is capable of capturing the entire load-deformation response of a concrete specimen under monotonic loading including softening. The new condition for crack penetration is developed based on a simple specimen configuration where a crack is driven towards an aggregate particle. Results from numerical simulations are implemented to relate the relative properties of both aggregate and matrix phases (represented by the characteristic length ratio) to their tensile strength ratio. It is shown that the tensile strength ratio between the aggregate and the matrix plays the dominant role in determining the penetration condition. Predictions based on this condition agree with direct tensile simulations using different specimen configuration.

Keywords: Crack-aggregate interaction; Numerical modeling; Crack propagation; Fracture mechanics; Material properties

1. Introduction

Generally, the mechanical properties of aggregate play a minor role in the mechanical behavior of normal strength concrete due to the weak interface between the aggregate and matrix phases. The weakness of the interface inhibits the achievement of composite action in normal strength concrete (e.g. [1,2]). However, current enhancement in matrix properties allows for the matrix and aggregate properties to be comparable. This is also associated with a considerable improvement in the interface properties leading to higher chances of achieving composite action. In such cases, as high strength concrete, it is more likely to have cracks penetrating the aggregate particles. Thus, the aggregate properties start to influence the composite behavior. In order to understand the role of the aggregate phase in these cases, the crack-aggregate interaction is investigated in this study.

There exist several analytical and numerical solutions for the problem of cracks located at or approaching an interface between dissimilar materials (e.g. [3–9]). These solutions are basically based on Linear Elastic Fracture Mechanics (LEFM). However, as concrete materials exhibit a considerable fracture process zone ahead of a crack tip, direct application of these models is not feasible.

In this study, a numerical model is used to simulate fracture in concrete materials with particular emphasis on studying the crack-aggregate interaction. Results from the numerical simulations are implemented to develop a new condition for predicting whether advancing cracks deflect at or penetrate the aggregate phase. For this purpose, a simple crack-aggregate configuration is used in which the crack has been driven towards an inclusion where the initial crack tip is far from the inclusion surface. A newly developed micromechanical model by Mohamed [10] has been used in the numerical simulation where nonlinear fracture mechanics concepts are implemented to describe the material properties. Further, many other simulations have been conducted to validate the predictions of the proposed condition for concrete samples under direct tensile mode. These samples are generated using the new micromechanical model.

* Corresponding author.

0958-9465/99/$ - see front matter
PII: S0958-9465(99)00016-5

2. The micromechanical model

It is now generally accepted that the macroscopic mechanical behavior of concrete materials is directly related to fracture processes at the microlevel. Therefore, several models have been proposed to model such behavior by simulating the concrete microstructure numerically using the finite element method. A common feature of most of these approaches is to randomly generate aggregate particles within a certain domain, however, they differ in the way the domain is discretized into finite elements. For instance, Roelfstra [11], Vonk [12], Stankowski [13] used continuum finite elements to discretize the concrete internal structure, while Bazant et al., [14] and Schlangen et al. [15] have used discrete elements in their discretization (truss and beam elements).

In the micromechanical model used in this investigation, the concrete internal structure is modeled as a three-phase material. The mechanical behavior of concrete is simulated numerically through the finite element method. The model considers tensile cracking at the microlevel as the only failure criterion associated with concrete fracture. Thus, truss elements are used as the basic element in the finite element mesh. The heterogeneity of the concrete internal structure is simulated through the randomization of aggregate particles. Further, the material properties are either randomized using a Gaussian distribution about the mean value through Monte Carlo simulation or assigned deterministically. As the aggregate particles are generated within the specimen boundaries, the three phases of the concrete internal structure can be identified, viz., the matrix, the aggregate and the interfaces between them. The process of simulation can be divided into four distinct steps.

(1) Random generation of the aggregate particles within the specified boundaries as ellipses. The information required in this step is the aggregate gradation curve, i.e. the number of particles for each size. The aggregate shape can be specified either with a fixed aspect ratio, or the aspect ratio can be randomized. The particles are allocated randomly starting with large ones. Each new particle is checked such that a minimum distance is maintained between the particles' boundaries to assure space for the matrix phase. Since it is beyond the computational means to consider all aggregate sizes, only particle sizes greater than 5 mm are considered. The process of aggregate generation is similar to that used by Bazant et al. [14]. However, generating ellipses, as used in this study, requires more complicated scheme.

(2) A finite element mesh is generated taking into account aggregate boundaries. The finite element mesh is generated as regular triangle elements and the elements' edges are considered as truss elements. After generating the finite element mesh, each element is identified according to its location (i.e. inside or outside the particles, or at the interface) as shown in Fig. 1.

(3) The constitutive relation of each element is assigned according to its location in the assembly as shown in Fig. 1. The constitutive relation of each element is constructed based on the smeared crack concept (e.g. [16,17]), where the input parameters for each phase are the tensile strength (f_t), the elastic modulus (E), and the fracture energy (G_F). The element length is implemented in the constitutive relation to arrive at a mesh-objective results. A schematic constitutive relation is shown in Fig. 2 where the strain at ultimate stress $\varepsilon p = ft/E$, and the strain at failure εu is defined as a function of G_F, f_t, and the element length L_m according to the stress-separation curve. For instance, in case of linear decay, $\epsilon u = 2G_F/f_t L_m$, while for exponential decay, $\varepsilon_u = [k/(1 - \exp(-k))]G_F/f_t L_m$. Upon unloading from an arbitrary point m in the softening part, the unloading strain ε_r is related to the strain at unloading ε_m through the relation $\varepsilon_r = \beta(\epsilon_m - \sigma_m/E)$. The factor β allows for modeling according to damage modeling (i.e. $\beta = 0$), plasticity modeling (i.e. $\beta = 1.0$), and other cases in between (i.e. $1.0 > \beta > 0$). A similar approach has been used by Roelfstra [11] and Dahlblom [16]. A full description of the different loading and unloading paths is available elsewhere ([10]).

(4) The last step of the simulation is to assemble the stiffness matrix according to the constitutive relation of each element and solve the generated equations. This has been accomplished using a nonlinear finite element scheme developed in this study. The displacement at certain prescribed nodes is assigned incrementally according to the boundary conditions of the problem in hand. For each increment, the Newton–Raphson iteration is implemented where the stiffness matrix is reas-

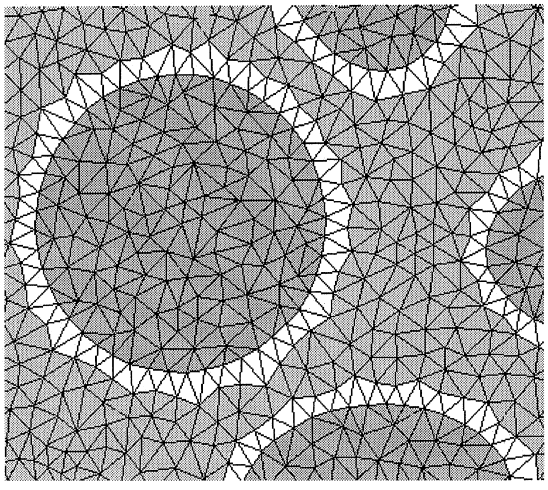

Fig. 1. Mesh details: dark gray represents aggregate phase, light gray represents matrix phase, and white represents interfaces.

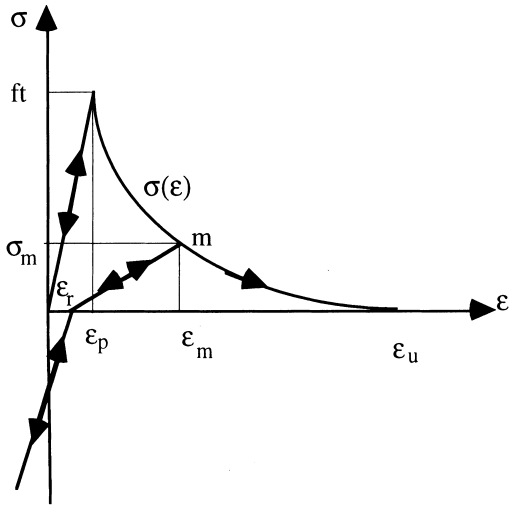

Fig. 2. Complete constitutive relation in tension.

sembled at each iteration according to any changes in the status of elements.

Several computer programs have been developed to accomplish each of the previous steps. A more detailed description of each step is available elsewhere ([10]). The model is capable of predicting the entire load-deformation response of concrete including softening, localization of deformation, and crack patterns at any loading stage. Also, the model is mesh-objective, i.e. the results of the simulation are independent of the finite element mesh fineness, provided that the mesh is fine enough to represent the heterogeneity of the internal structure as shown in Fig. 3. This simulation is for the same material properties and aggregate generation for a 100 × 100 mm specimen loaded in uniaxial tension.

The new micromechanical model shares some aspects with other existing models which use discrete elements, and contrast with others. For instance, the random particle model by Bazant et al. [14] shows a realistic prediction of the concrete tensile response under direct tensile loading. However, this model does not consider the interfacial zone between the aggregate and the matrix while this model does. The interfacial zone properties have been proven to have a considerable effect on the concrete behavior [1,2]. On the other hand, the beam model by Schlangen et al. [15] follows elastic-brittle fracture rules without considering the softening response which may have a direct effect on the objectivity of the results ([18]). Further, the concept of removing the element from the mesh as the element fractures does not allow for unloading modeling.

The new micromechanical model is implemented in this study to establish a new condition for crack penetration into aggregate particles. Furthermore, the application of this condition to high strength concrete is investigated.

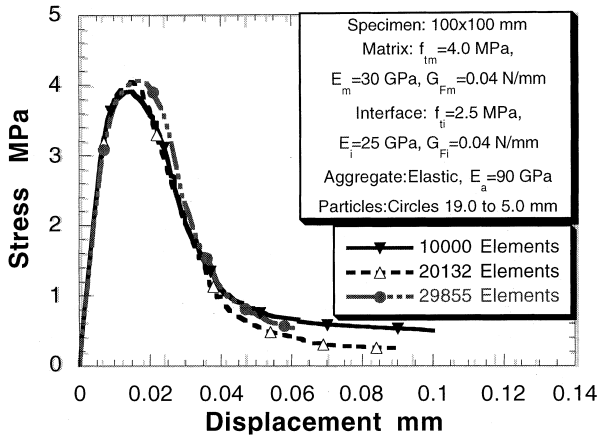

Fig. 3. Checking mesh-objectivity for a three-phase material: three simulations using different number of elements.

3. Crack-aggregate interaction:

3.1. Specimen configuration

A simple specimen configuration, similar to that used by Tan et al. [19] for studying the interface fracture energy, has been used to study the crack-aggregate interaction as shown in Fig. 4. The dimensions of the specimen are chosen such that the location of the inclusion does not affect the stress intensity factor at the initial crack tip. Thus, the driven crack feels the inclusion as it advances. This condition is preserved to simulate the scenario of cracks approaching the aggregate particles in concrete materials. This will ensure that the

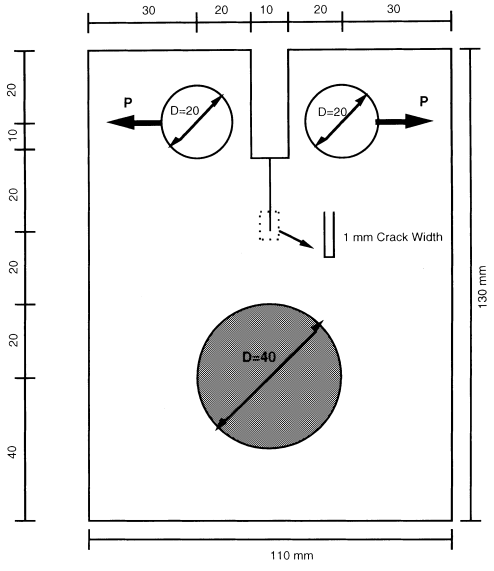

Fig. 4. Specimen configuration for the crack-aggregate interaction.

inclusion properties will not affect the initial propagation of the crack. The effect of the relative location of the inclusion on the crack tip stress intensity factor is explained elsewhere (e.g., Rongshun, et al., Patton et al., and [9]). After several numerical simulations for different inclusion locations, the dimensions shown in Fig. 4 have been chosen. As shown in Fig. 5, varying the elastic modulus of the inclusion reveals nearly identical results. In these simulations, the aggregate phase is considered elastic, and the interface properties (i.e. tensile strength f_{ti}, elastic modulus E_i, and fracture energy G_{Fi}) are considered as 80% of the corresponding matrix properties, i.e. good bonding as will be demonstrated in the next part of this section. This configuration will be used throughout.

3.2. Effect of interface properties

Before investigating the conditions for crack penetration into the aggregate phase, the effect of the interface properties (i.e. f_{ti}, E_i, G_{Fi}) is first studied. Changing the ratio (r) between the interface properties and the corresponding matrix properties, while keeping the aggregate phase elastic, reveals different responses as shown in Fig. 6. Model predictions show that the load carrying capacity of the specimen increases as the ratio r approaches 1.0. A considerable reduction in the load carrying capacity is predicted if r falls below a ratio of 0.6.

The crack patterns for these simulations are shown in Fig. 7 corresponding to ultimate load and end of simulations. In all crack patterns, thin lines represent softening cracks and thick lines represent full cracks. In all simulations, the initial crack starts to grow only after reaching the ultimate load. Further, the crack patterns corresponding to the ultimate load reveal interesting findings regarding the fracture process zone ahead of the crack tip. For very low interface properties ($r = 0.4$), intensive cracks exist at the interface, while for higher r values of 0.6 and lower, while higher values are associated with final matrix crack deflecting away from the inclusion.

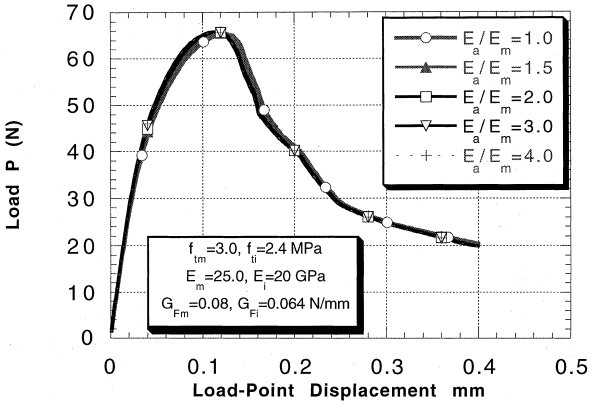

Fig. 5. Crack-aggregate interaction specimen responses as influenced by changing aggregate elastic modulus.

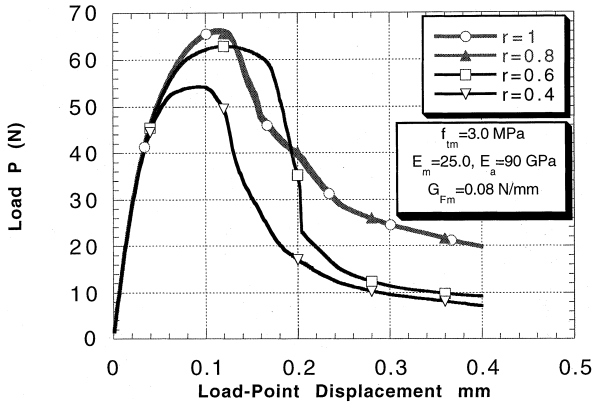

Fig. 6. Effect of interface properties on the specimen response.

3.3. Parameters affecting crack penetration into the aggregate phase

It is well known that cracks penetrate the aggregate phase in cases where the interface properties are close to the matrix properties, as in high strength concrete. Therefore, in order to concentrate this investigation on studying the conditions of crack penetration into the aggregate, the possibility that the initial crack propagates through the interface is eliminated. This is accomplished by considering the interface properties as 90% of the matrix properties. Thus, only two possibilities exist for crack propagation: 1) either penetrating the inclusion, or 2) deflecting in the matrix away from the inclusion. The aggregate properties considered are the elastic modulus (E_a), the tensile strength (f_{ta}), and the fracture energy (G_{Fa}). These parameters are changed as a ratio of the corresponding matrix properties, E_m, f_{tm}, and G_{Fm}, respectively (i.e. E_a/E_m, f_{ta}/f_{tm}, and G_{Fa}/G_{Fm}). Three values have been chosen for E_a/E_m: 3.0, 2.0, and 1.0. Concurrently, for each ratio of E_a/E_m, the tensile strength ratio f_{ta}/f_{tm} has been changed in 0.5 increment starting with the ratio of 0.5, i.e. $0.5, 1.0, 1.5, \ldots$ etc. until the mode of penetration changes. At the same time, for certain ratios of E_a/E_m and f_{ta}/f_{tm}, a range of values for G_{Fa}/G_{Fm} have been investigated until either the mode of penetration changes, or the ratio G_{Fa}/G_{Fm} becomes unrealistic. Results of these simulations will be presented in the following sections. Furthermore, many other simulations have been investigated using values of $f_{ta}/f_{tm} = 0.6$, 0.75, 0.8, 1.2, 1.25, and 3.0. These results are presented only as data points in the analysis part of this section.

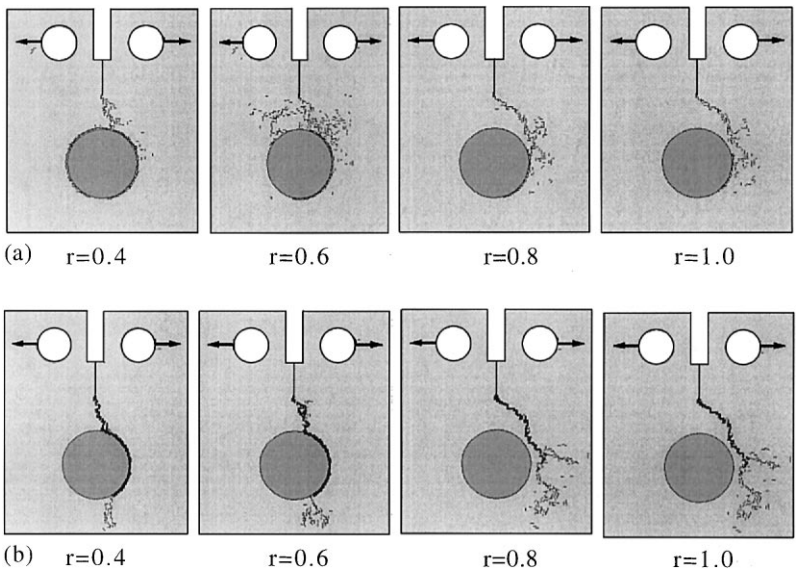

Fig. 7. Crack patterns for the effect of interface properties: (a) cracking patterns at peak load for different r values; (b) cracking patterns at the end of simulations for different r values.

3.4. (a) Elastic moduli ratio $E_a/E_m = 3.0$

Shown in Fig. 8 are the responses resulting from changing G_{Fa}/G_{Fm} from 0.25 to 8.0 for $f_{ta}/f_{tm} = 0.5$. All simulations result in crack penetration into the aggregate. Also as shown in the same figure, the predicted peak load is independent of the fracture energy ratio, while the ductility of the specimen in the post peak part enhances considerably as the fracture energy ratio increases. However, some of the G_{Fa}/G_{Fm} ratios are unrealistic and are included only to examine whether the effect of increasing this parameter can alter the penetration mode. On the other hand, if f_{ta}/f_{tm} increases to 1.0, and as the ratio G_{Fa}/G_{Fm} approaches 1.0, predictions show that no penetration occurs beyond this limit as depicted from Fig. 9. In non-penetrating cases, the post peak response shows higher ductility than the cases where penetration occurs. Ultimate load, however, remains constant.

If the tensile strength ratio, f_{ta}/f_{tm}, increases to 1.5, no crack penetration occurs irrespective of how small the fracture energy ratio, G_{Fa}/G_{Fm}, becomes as shown in Fig. 10. In this case, all simulations reveal identical responses.

3.5. (b) Elastic moduli ratio $E_a/E_m = 2.0$

Similar trends are observed as for the case of $E_a/E_m = 3.0$ for $f_{ta}/f_{tm} = 0.5$ with penetrating crack for all G_{Fa}/G_{Fm} values. For cases of $f_{ta}/f_{tm} = 1.0$, the limit for crack penetration is reached at $G_{Fa}/G_{Fm} = 1.0$ as shown

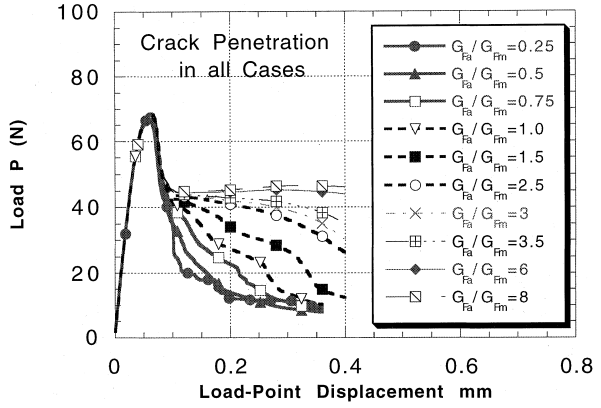

Fig. 8. Effect of the aggregate fracture energy on the specimen response ($E_a/E_m = 3.0$, $f_{ta}/f_{tm} = 0.5$).

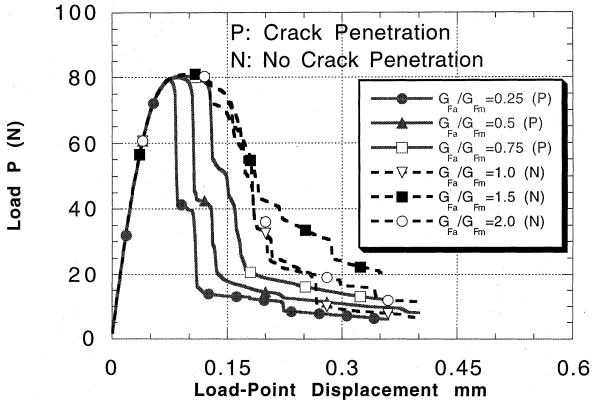

Fig. 9. Effect of the aggregate fracture energy on the specimen response ($E_a/E_m = 3.0$, $f_{ta}/f_{tm} = 1.0$).

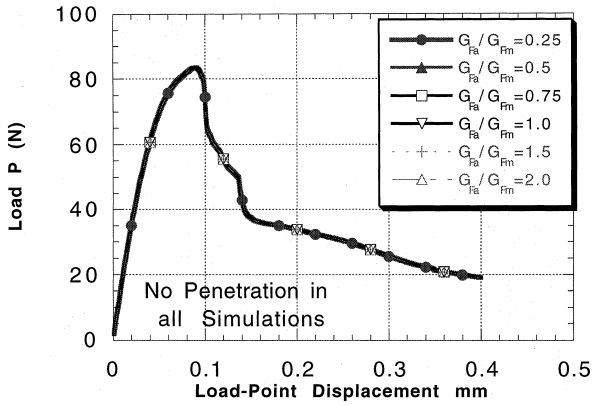

Fig. 10. Effect of the aggregate fracture energy on the specimen response ($E_a/E_m = 3.0$, $f_{ta}/f_{tm} = 1.5$).

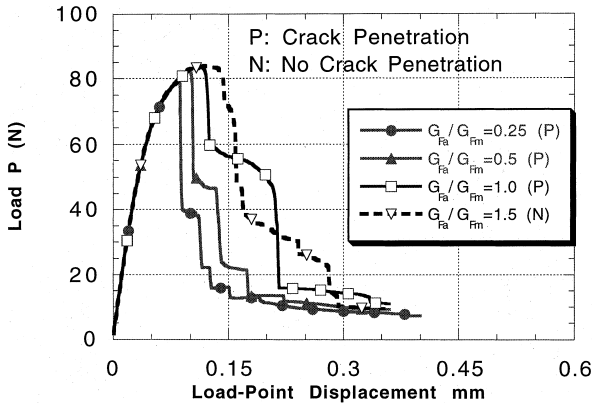

Fig. 12. Effect of the aggregate fracture energy on the specimen response ($E_a/E_m = 1.0$, $f_{ta}/f_{tm} = 1.5$).

in Fig. 11. Also, for $f_{ta}/f_{tm} = 1.5$, no penetration occurs irrespective of the G_{Fa}/G_{Fm} values.

3.6. (c) Elastic moduli ratio $E_a/E_m = 1.0$

In this category, $f_{ta}/f_{tm} = 0.5$ and 1.0 show that the crack will also penetrate, irrespective of the G_{Fa}/G_{Fm} values, with responses very similar to the ones before. However, for $f_{ta}/f_{tm} = 1.5$, penetration occurs up to a G_{Fa}/G_{Fm} value of 1.0, after which no penetration occurs as shown in Fig. 12. Higher values of f_{ta}/f_{tm}, i.e. 2.0, have been tested. These results reveal that penetration occurs only for very low ratio of $G_{Fa}/G_{Fm} = 0.25$, while no penetration has been predicted for higher values as depicted from Fig. 13.

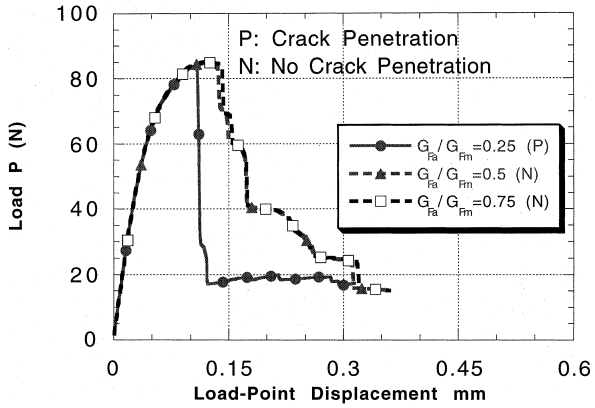

Fig. 13. Effect of the aggregate fracture energy on the specimen response ($E_a/E_m = 1.0$, $f_{ta}/f_{tm} = 2.0$).

3.7. Analysis of the predicted results

Based on the previous findings, it is evident that the tensile strength ratio, f_{ta}/f_{tm}, plays the most significant role in determining whether a crack will penetrate an aggregate or not. Therefore, this ratio has been chosen as the main variable in the analysis. The fracture energy ratio, G_{Fa}/G_{Fm}, plays a less significant role, while the elastic moduli ratio, E_a/E_m, plays the least important role.

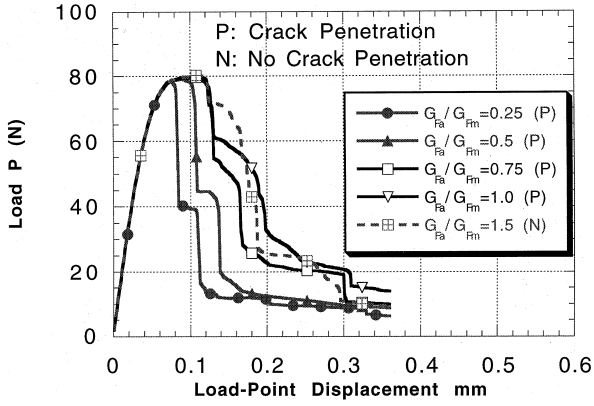

Fig. 11. Effect of the aggregate fracture energy on the specimen response ($E_a/E_m = 2.0$, $f_{ta}/f_{tm} = 1.0$).

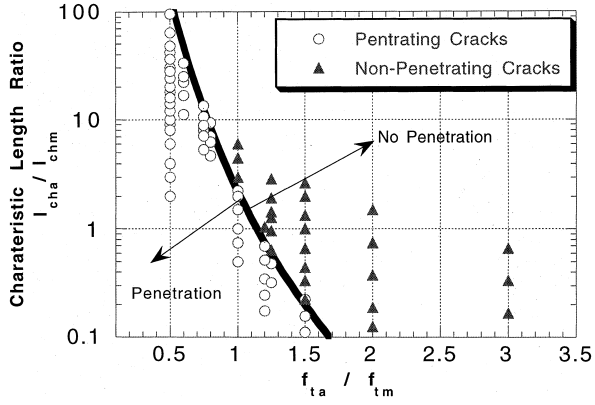

Fig. 14. Characteristic length ratio vs tensile strength ratio and the condition for crack penetration.

In order to determine a condition for crack penetration, several combinations are investigated for the considered parameters. Surprisingly, the most efficient way to express this condition is found to be the relation between the characteristic length ratio between the aggregate and the matrix, l_{ch_a}/l_{ch_m}, and the tensile strength ratio, f_{ta}/f_{tm}, as shown in Fig. 14. In this context, the characteristic length is defined as $l_{ch} = EG_F/f_t^2$. The data points in this figure include previous simulations and many other simulations whose load-deformation responses are not shown. The condition for crack penetration is given by the following inequalities,

$$\begin{aligned} &\text{Penetrating}: \ l_{ch_a}/l_{ch_m} \leqslant 2.25(f_{ta}/f_{tm})^{-6.0}, \\ &\text{Non-penetrating}: \ l_{ch_a}/l_{ch_m} > 2.25(f_{ta}/f_{tm})^{-6.0}. \end{aligned} \quad (1)$$

These inequalities give the condition for crack penetration for the given configuration, where the crack is driven symmetrically towards the middle of an aggregate particle. However, in reality, a crack might hit the aggregate particles at any angle and location. Furthermore, cracks might initiate from the interface of the aggregate particle itself. Thus, the application of the condition in Eq. (1) should be taken with caution. Despite this, the equation gives a good prediction for crack penetration as will be discussed later.

The impact of crack penetration on the ultimate load has been found to be significant as shown in Fig. 15 for practical values of the material properties used. It is evident that crack penetration always results in a lower ultimate load as compared to non-penetrating cracks. At the same time, for practical values of G_{Fa}/G_{Fm}, the penetrating crack shows a sudden drop in the load-deformation response beyond the peak load, while a non-penetrating crack reveals more ductile behavior. Also, from Fig. 15, the ratio of the aggregate to matrix tensile strength plays the most significant role in determining the ultimate load. This is a crucial factor in producing high strength concrete, as the aggregate properties start to play a role in determining the concrete load-carrying capacity unlike normal strength concrete.

The crack patterns associated with the previous simulations show three distinct patterns as illustrated in Fig. 16. For a non-penetrating crack, the initial crack propagates in the matrix away from the aggregate, while for penetrating cracks, with practical G_{Fa}/G_{Fm} ratio (i.e. up to 1.5), the crack extends in a tortuous manner within the aggregate boundary. However, for penetrating cracks with high G_{Fa}/G_{Fm} (i.e. 1.5 and up) even at the end of the simulation, the initial crack propagates until hitting the aggregate boundaries. The crack in these cases possesses a large fracture process zone inside the aggregate particle having softening cracks. It is worth mentioning that both the predicted load-deformation response and crack patterns follow similar trends as observed experimentally by Tan et al. [7].

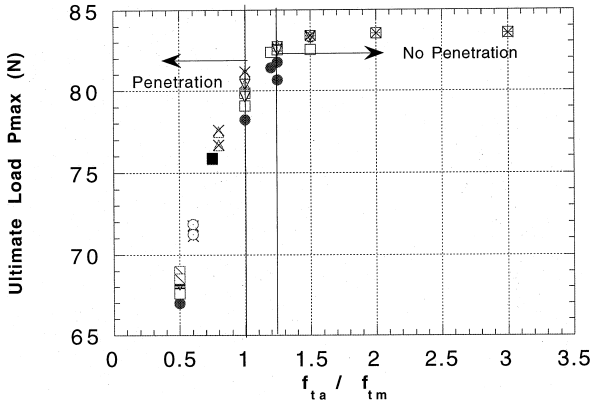

Fig. 15. Ultimate load of the specimen as influenced by the increase in tensile strength ratio and the mode of penetration.

4. Numerical validation of Eq. (1)

For high strength concrete, there is a high probability that cracks penetrate into the aggregate phase. In order

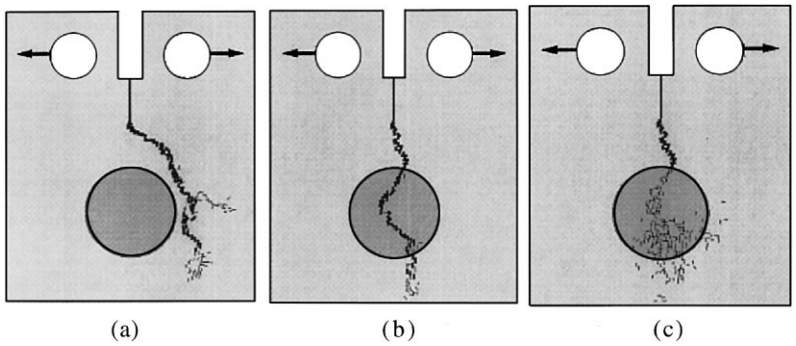

Fig. 16. Typical crack patterns for all simulations: (a) non-penetrating crack; (b) penetrating crack; (c) penetrating crack with high aggregate fracture energy.

to examine that, in lieu of the findings discussed above, several numerical simulations have been carried out. In all simulations, the ratio of the elastic moduli of aggregate to matrix is kept constant at 3.0, while three tensile strength ratios have been considered (viz., 0.5, 1.0, and 1.5). For each tensile strength ratio, the fracture energy of aggregate to matrix G_{Fa}/G_{Fm}, has been changed in a value of 0.5 increment starting with 0.5 until the mode of failure changes (i.e., the crack penetration). All the interface properties are held constant at 90.0% of the matrix properties. They are $f_{tm} = 6.0$ MPa, $G_{Fm} = 0.06$ N/mm, and $E_m = 30.0$ GPa.

Model predictions for the first case, where $f_{ta}/f_{tm} = 0.5$ are shown in Fig. 17(a) for different G_{Fa}/G_{Fm} ratios. For these simulations, the cracks are penetrating the aggregate. In fact, due to the lower tensile strength of the aggregate phase, the cracks even initiate from the aggregate phase and propagate toward the matrix. Of interest is that, as the aggregate tensile strength becomes lower than the matrix tensile strength, the aggregate phase becomes lower than the matrix tensile strength, the aggregate phase becomes the controlling parameter in determining the tensile strength of concrete.

Despite the fact that the aggregate fracture energy has a negligible effect on the ultimate load value, it influences the post-peak part of the response significantly. Typical crack patterns are shown in Fig. 17(b) for the cases of $G_{Fa}/G_{Fm} = 0.5$ and 2.0.

If, on the other hand, the aggregate tensile strength increases to that of the matrix tensile strength, the behavior starts to change dramatically as shown in Fig. 18(a). The tensile strength of concrete is now comparable to the matrix tensile strength, and the post-peak part becomes steeper. Only two responses are shown. The first one corresponds to $G_{Fa}/G_{Fm} = 0.5$, where considerable crack penetration occurs. However, when the G_{Fa}/G_{Fm} ratio increases to 1.0, the interface cracking dominates the behavior as in normal strength concrete. Shown in Fig. 18(b) are the crack patterns associated with these simulations. This case corresponds to a composite material with the two phases having the same tensile strength and fracture energy but different elastic moduli.

In cases where the tensile strength of the aggregate phase exceeds that of the matrix, the aggregate phase plays less and less role in the concrete tensile behavior. As shown in Fig. 19(a), the tensile response is almost identical for different G_{Fa}/G_{Fm} ratios, as long as the tensile strength of the aggregate phase is 1.5 times the matrix tensile strength. For a low G_{Fa}/G_{Fm} ratio

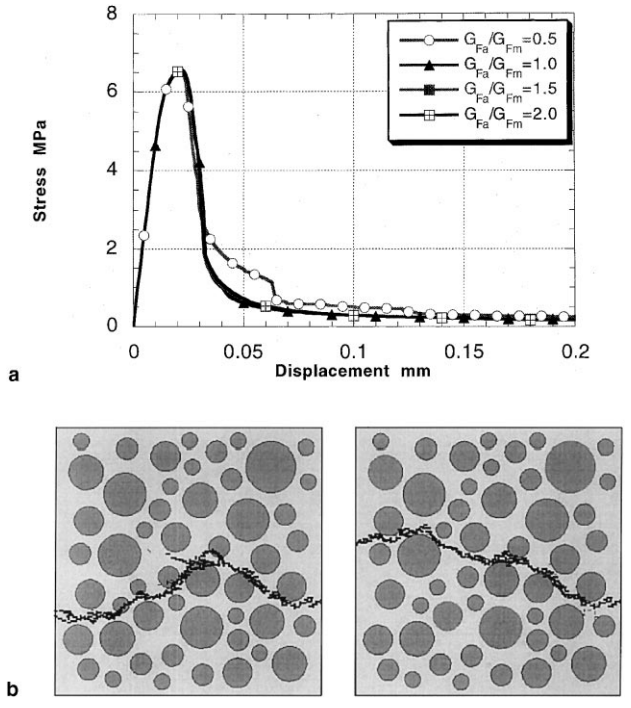

Fig. 17. Response and crack patterns for tensile simulation with $f_{ta}/f_{tm} = 0.5$: (a) tensile stress–displacement as influenced by the change in the fracture energy ratio between aggregate and matrix ($E_a/E_m = 3.0$ and $f_{ta}/f_{tm} = 0.5$); (b) crack patterns at the end of simulation for $G_{Fa}/G_{Fm} = 0.5$ and 2.0.

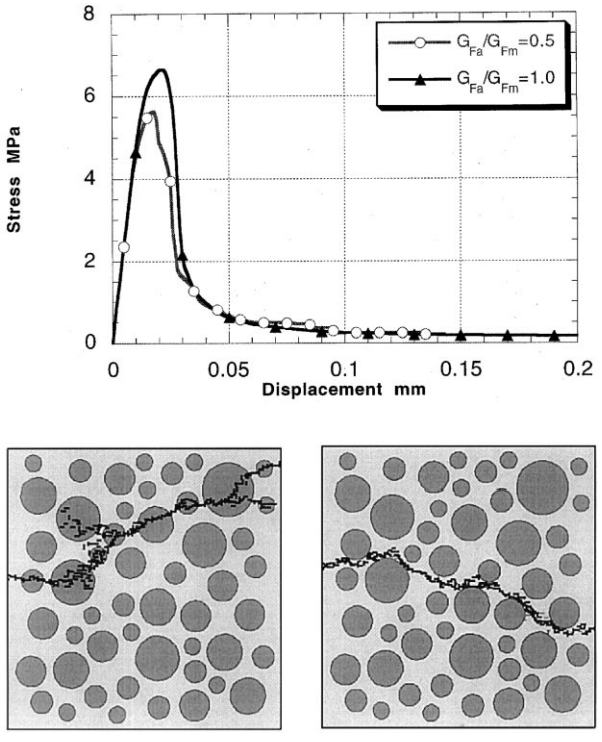

Fig. 18. Response and crack patterns for tensile simulation with $f_{ta}/f_{tm} = 1.0$: (a) tensile stress–displacement as influenced by the change in the fracture energy ratio between aggregate and matrix ($E_a/E_m = 3.0$ and $f_{ta}/f_{tm} = 1.0$); (b) crack patterns at the end of simulation for $G_{Fa}/G_{Fm} = 0.5$ and 1.0.

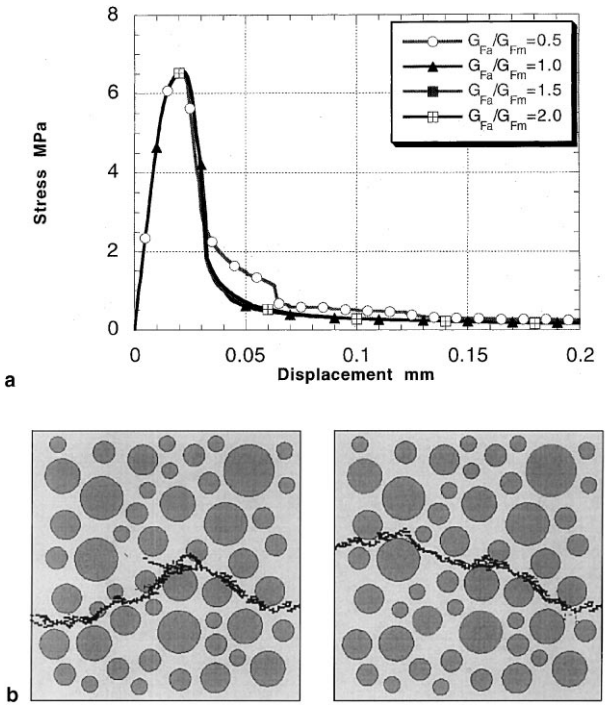

Fig. 19. Response and crack patterns for tensile simulation with $f_{ta}/f_{tm} = 1.5$: (a) tensile stress–displacement as influenced by the change in the fracture energy ratio between aggregate and matrix ($E_a/E_m = 3.0$ and $f_{ta}/f_{tm} = 1.5$); (b) crack patterns at the end of simulation for $G_{Fa}/G_{Fm} = 0.5$ and 2.0.

of 0.5, the response is somewhat different after the peak load due to some crack penetration as shown in Fig. 19(b).

A summary of all the direct tensile simulations is given in Table 1, together with the prediction of crack penetration according to Eq. (1). As depicted from this table, despite the difference in the configuration between the crack-aggregate interaction specimen and the direct tensile simulation specimen, Eq. (1) successfully predicts the crack penetration in the direct tensile simulation.

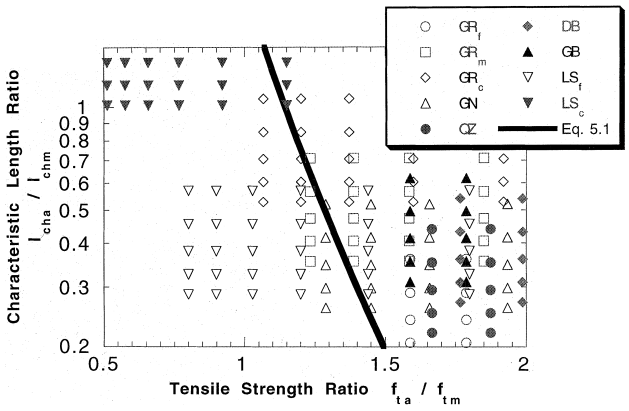

Fig. 20. Penetration condition for different types of aggregate and matrix based on the condition proposed by Eq. (1) (aggregate symbols are explained in Table 2).

5. Application of Eq. (1) to different aggregate types

In order to examine the predictions of Eq. (1) to different aggregate types, the experimental data reported by Hassanzadeh [20] as listed in Table 2 are considered. This table lists the properties of different aggregate types. A range of matrix tensile strengths of 3.0–9.0 MPa and characteristic lengths ranging from 100 to 200 mm are considered. Combinations of the experimentally documented values for aggregate tensile strength and characteristic lengths, with a variation of the assumed matrix properties range are taken into account. The part of the results close to the equation prediction, with practical aggregate/matrix ratios, is shown in Fig. 20, together with the prediction of Eq. (1). According to the model prediction, there is a high probability that limestone aggregate (both fine and coarse grained types) will result in crack penetration, while a very high strength matrix is needed for coarse or medium grained granite for crack penetration. On the other hand, quartz aggregate has less tendency for crack propagation.

Comparison of the previous predictions to actual experimental data is rather difficult due to the scarcity of

Table 1
Comparison between tensile simulation and Eq. (1) predictions ($E_a/E_m = 3.0$)

f_{ta}/f_{tm}	G_{Fa}/G_{Fm}	l_{ch_a}/l_{ch_m}	$2.25(f_{ta}/f_{tm})^{-6.0}$	Simulation prediction	Eq. (1) prediction
0.5	0.5	6.0	144	P	P
0.5	1.0	12.0	144	P	P
0.5	1.5	18.0	144	P	P
0.5	2.0	24.0	144	P	P
1.0	0.5	1.5	2.25	P	P
1.0	1.0	3.0	2.25	N	N
1.5	0.5	0.667	0.198	N	N
1.5	1.0	1.333	0.198	N	N
1.5	1.5	2.000	0.198	N	N
1.5	2.0	2.667	0.198	N	N

P = crack penetration, N = no penetration.

Table 2
Fracture mechanical properties of rocks ([8])

Rock	f_c (MPa)	f_{st} (MPa)	f_{net} (MPa)	E_d (GPa)	E_s (GPa)	G_{Fa} (N/mm)	l_{cha} (mm)
GR_f	233.7	14.3	15.6	79.3	59.1	0.1244	36.0
GR_m	160.0	11.1	11.8	79.9	63.3	0.1349	71.0
GR_c	153.4	9.6	13.5	73.5	61.2	0.1590	106.0
G_N	183.3	11.6	12.0	72.6	59.4	0.1156	52.0
QZ	332.0	15.0	13.9	76.0	60.2	0.1628	44.0
DB	311.9	15.9	17.2	123.3	104.6	0.1287	54.0
GB	256.7	14.3	16.9	104.1	93.7	0.1336	62.0
LS_f	160.4	7.2	10.6	67.0	57.8	0.0506	57.0
LS_c	51.9	4.6	6.5	64.5	52.3	0.0743	203.0

GR_f, GR_m, and GR_c = fine, medium, and coarse grained granite, respectively; GN = gneiss; QZ = quartzite; DB = diabase; GB = gabro; and LS_f and LS_c = fine and coarse grain limestone. f_c, f_{st}, f_{net}, E_d, E_s, G_{Fa}, and l_{cha} are compressive strength, splitting strength, flexural strength, dynamic modulus, static modulus, fracture energy, and characteristic length, respectively.

data regarding tensile testing. However, as the condition given by Eq. (1) is developed for a crack driven towards an inclusion, this condition can be extended to other modes. For instance, under uniaxial compressive loading, cracks develop in the loading direction and propagate towards inclusions. Thus, a scenario similar to the one considered in this study emerges. For example, Mehta et al. [1] studied the effect of aggregate type on concrete compressive strength. They reported that the failure surface penetrates aggregates for both granite and limestone. However, quartz aggregates show no sign of crack penetration and cracks are mainly found in the interface zone. The model predictions for these types of aggregates are in agreement with experimental findings. However, they also reported crack penetration in the case of diabase aggregate, which the model does not predict. The properties of diabase reported in Table 2 suggest that it is the strongest aggregate tested. However, these properties vary from one site to another and they may not be considered typical. Despite the fact that the configuration considered is far from comparison with compressive loading, the condition provided by Eq. (1) shows reasonable agreement with experimentally observed crack penetration.

6. Conclusions

A new condition for crack penetration into the aggregate phase in concrete materials has been presented based on a newly developed micromechanical model. The condition relates the ratio between the characteristic lengths of aggregate to matrix phases to their tensile strength ratio. The predictions of the proposed condition is compared to tensile simulations and experimentally observed crack penetration under compressive loading. The following conclusions can be drawn.

(1) Enhancing the interface properties, as compared to matrix properties, has a direct impact on achieving composite action in concrete materials. If the interface properties exceed 60% of the corresponding matrix properties, cracks might deflect away from the aggregate instead of being trapped in the interfacial zone.

(2) If the interfacial properties are enhanced, to a level of 80% or more of the corresponding matrix properties, the aggregate properties start to play a significant role in the mechanical behavior of concrete.

(3) The tensile strength ratio between the aggregate and matrix phases is the most significant factor in determining the possibility of crack penetration. The fracture energy ratio is the second most important parameter, followed by the moduli ratio.

(4) Numerical simulations reveal a significant impact of crack penetration on the ultimate load capacity for the configuration considered. Higher peak loads are predicted for non-penetrating cracks.

(5) The condition of crack propagation represented by Eq. (1) successfully predicts crack penetration in numerical simulations for direct tensile specimens which are quite different than the configuration used to develop the condition.

(6) A simple comparison is held between the predictions of crack penetration based on Eq. (1) and some experimental observations for concrete tested in uniaxial compression. Despite these differences, Eq. (1) reveals some predictions in agreement with the experimental work observations.

Acknowledgements

The authors would like to thank the Center for Parallel Computing at the University of Michigan, Ann Arbor, for providing the computational means to conduct the numerical simulation part of this research.

References

[1] Mehta PK, Aïtcin PC. Microstructural basis of selection of materials and mix proportions for high strength concrete. In:

Weston TH. editor, High Strength Concrete, Second International Symposium, ACI SP-121, 1990:265–79.
[2] Aïtcin PC, Neville A. High performance concrete demystified. Concrete International 1993;15(1):21–6.
[3] He Ming-Yuan, Hutchinson JW. Crack deflection at an interface between dissimilar elastic materials. International Journal of Solids and Structures 1989;25(9):1053–67.
[4] Atkinson T. The interaction between a crack and an inclusion. International Journal of Engineering Science 1972;10:127–36.
[5] Cook TS, Erdogan F. Stress in bonded materials with a crack perpendicular to the interface. International Journal of Engineering Science 1972;10:677–97.
[6] Li R, Chudnovsky A. Stress intensity factor Green's function for a crack interacting with a circular inclusion. International Journal of Fracture 1994;67(2):169–77.
[7] Patton EM, Santare MH. Crack path prediction near an elliptical inclusion. Engineering Fracture Mechanics 1993;44(2):195–05.
[8] Patton EM, Santare MH. The effect of a rigid elliptical inclusion on a straight crack. International Journal of Fracture 1990;46(1):71–9.
[9] Santare MH, O'Toole BJ, Patton EM. Two-dimensional crack inclusion interaction effects. Analysis and experiments. Journal of Pressure Vessel Technology, ASME, 1991;113(3):392–97.
[10] Mohamed Ashraf R. Micromechanics of concrete behavior and progressive failure under static loading. Ph.D. thesis. Ann Arbor: University of Michigan, 1997:346.
[11] Roelfstra PE. Simulation of strain localization process with numerical concrete. In: Mazars J, Bazant ZP. editors. Cracking and Damage. London: Elsevier, 1989:79–90.
[12] Vonk R. Softening of Concrete Loaded in Compression, Ph.D. Thesis. The Netherlands: Eindhoven, 1992.
[13] Stankowski T. Numerical Simulation of Progressive Failure in Particle Composites, Ph.D. Thesis. University of Colorado, 1990.
[14] Bazant ZP, Tabbara MR, Kazemi MT, Pijaudier-Cabot G. Random particle model for fracture of aggregate or fiber composites. Journal of Engineering Mechanics 1990;116(8):1686–705.
[15] Schlangen E. van Mier JGM. Experimental and numerical analysis of micro mechanisms of fracture of cement based composites. Journal of Cement and Concrete Composites 1992;14:105–18.
[16] Dahlblom O, Ottosen NS. Smeared crack analysis using generalized fictitious crack model. Journal of Engineering Mechanics 1990;116(1)55–76.
[17] Bazant ZP, Oh BH. Crack band theory for fracture of concrete. Materials and Structures, RILEM 1983;16:155–77.
[18] Schlangen E. Computational aspects of fracture simulations with lattice models. In: Wittmann FH. editor. Fracture Mechanics of Concrete Structures, Proceedings FRAMCOS-2, AEDIFICATIO Publishers, 1995:913–28.
[19] Tan DM, Tschegg EK, Rotter H, Krinchner HOK. Cracks at mortar-stone interfaces. Acta Metallurgica 1995;43(10): 3701–07.
[20] Hassanzadeh M. Fracture mechanical properties of rocks and mortar/rock interfaces. In: Microstructure of Cement-Based Systems/Bonding and Interfaces in Cementitious Materials,' Materials Research Society, Symposium Proceedings, vol. 370. Pittsburgh, PA: Materials Research Society, 1995:377–86.